Ferroelectric soft mode of polar ZnTiO_{3} investigated by Raman spectroscopy at high pressure

J. Ruiz-Fuertes, B. Winkler, T. Bernert, L. Bayarjargal, W. Morgenroth, M. Koch-Müller, K. Refson, V. Milman, and N. Tamura

Phys. Rev. B **91**, 214110 — Published 22 June 2015

DOI: 10.1103/PhysRevB.91.214110

Ferroelectric soft mode of polar $ZnTiO_3$ investigated by Raman spectroscopy at high pressure

J. Ruiz-Fuertes,[1,*] B. Winkler,[1] T. Bernert,[2] L. Bayarjargal,[1] W. Morgenroth,[1] M. Koch-Müller,[3] K. Refson,[4] V. Milman,[5] and N. Tamura[6]

[1] *Geowissenschaften, Goethe-Universität, Altenhöferallee 1, 60438 Frankfurt am Main, Germany*
[2] *Max-Planck-Institut für Kohlenforschung, Kaiser-Wilhelm-Platz 1, D-45470 Mülheim a. d. Ruhr, Germany*
[3] *GFZ Potsdam, Sektion 3.3, Telegrafenberg, 14473 Potsdam, Germany*
[4] *Dept. of Physics, Royal Holloway, University of London Egham, Surrey, TW20 0EX, United Kingdom*
[5] *Dassault Systèmes BIOVIA, 334 Science Park, Cambridge CB4 0WN, United Kingdom*
[6] *Advanced Light Source, Berkeley, CA 94720, USA*

(Dated: June 1, 2015)

In this work we explore the vibrational behavior and stability of ferroelectric $ZnTiO_3$ under high pressure by Raman spectroscopy and second harmonic generation (SHG) measurements. *Ab initio* lattice dynamics calculations have been employed to solve a controversy concerning the phonon-dispersion relations of $ZnTiO_3$ and to carry out an assignment of the Raman modes. A ferroelectric to paraelectric phase transition has been observed both by Raman spectroscopy and SHG at 20.8 GPa. Contrary to $LiNbO_3$, the ferroelectric soft mode of $ZnTiO_3$ has been found to be the $A_1(2)$ and not the $A_1(1)$ mode. The calculated eigenvectors show that the $A_1(2)$ mode of ferroelectric $ZnTiO_3$ is an antiphase vibration of the Ti atom against the oxygen framework, similarly to the soft modes observed in ferroelectric perovskites. The SHG signal of $ZnTiO_3$ has been found to be independent of the grain-size below the phase transition, indicating that $ZnTiO_3$ is a phase-matchable compound.

PACS numbers: 77.80.B-, 78.55.Ap, 42.65.Ky

I. INTRODUCTION

Non-linear optic behavior, piezoelectricity, pyroelectricity, and spontaneous polarization make ferroelectric materials of great technological importance [1–4]. Applications as ferroelectric random access memories (FRAM) [5] or as piezoactuators in microelectromechanical systems such as scanning probe microscopes [6, 7], are examples of their industrial relevance. Lead-based perovskites with a high-ferroelectic polarization have therefore been employed in many applications despite concerns regarding the impact of lead-bearing compounds on the environment [5, 8, 9]. In order to minimize the environmental impact, lead-free perovskite-related ABO_3 polar oxides are currently investigated extensively [10–13]. In this context, the recent high-pressure and high-temperature synthesis of polar zinc titanate ($ZnTiO_3$) [12] with an estimated spontaneous polarization of 75 μC/cm^2, which is similar to that of $PbTiO_3$, and a Second Harmonic Generation (SHG) signal 24 times as intense as that of $ZnSnO_3$ [10], has been a breakthrough in this search.

Polar $ZnTiO_3$ is isostructural to $LiNbO_3$ (space group $R3c$) with both cations being octahedrally coordinated in a three-dimensional corner-sharing octahedra perovskite (Pv)-like framework. In this structure both cations shift along the trigonal c-axis, thereby producing a spontaneous polarization which is enhanced by a second order Jahn-Teller distortion due to the Ti^{4+} (d^0). In terms of designing and developing possible applications based on $LiNbO_3$ (LN)-type $ZnTiO_3$, its ferroelectric instability needs to be understood.

The paraelectric parent structure of $ZnTiO_3$ is the ilmenite (Il)-type phase (space group $R\overline{3}$), which is the stable phase at ambient conditions. Both the LN-type and the Il-type structures are related by a zone-center ferroelectric mode that involves the displacement of the cations [14]. However, the LN-type to Il-type transformation requires octahedral rotations which are hindered due to anion-anion contacts for compounds with small tolerance factors [14]. Instead, LN-type $ZnTiO_3$ undergoes a phase transition to an orthorhombic (space group $Pmna$) Pv-type phase by an order-disorder phase transition [15–17]. Several studies on other LN-type ferroelectrics, such as LN-type $MnTiO_3$ [15] or LN-type $PbNiO_3$ [18], confirm this model.

Ab initio calculations predict the phase transition of LN-type $ZnTiO_3$ to the Pv-type structure at around 16 GPa [12]. Postnikov et al. [19] have shown in $LiNbO_3$ that the lowest frequency Raman $A_1(1)$ ferroelectric mode polarized along the threefold axis (c-axis) is unstable against an off-center displacement along this direction [20] and shows pressure-induced softening [21, 22]. Although the ferroelectric mode is not responsible for the LN-type to Pv-type phase transition due to the order-disorder character of the transition, identifying this mode in LN-type $ZnTiO_3$ is a prerequisite for understanding its ferroelectric behavior. In this work we have studied the ferroelectric instability of the recently discovered LN-type $ZnTiO_3$ by means of Raman spectroscopy and second harmonic generation (SHG) at ambient temperature and high pressures. We have performed an assignment of its Raman modes and investigated its ferroelectric soft

*Electronic address: ruiz-fuertes@kristall.uni-frankfurt.de

mode on the basis of *ab initio* lattice-dynamical calculations.

II. EXPERIMENTAL DETAILS

LN-type $ZnTiO_3$ was synthesized in powder form using pure Il-type $ZnTiO_3$ [23] sealed inside a platinum capsule at 16.5 GPa and 1150 °C in a multi-anvil press for 38 minutes following the work by Inaguna et al. [12]. The multi-anvil experiment was performed at GFZ Potsdam with a 10/5-assembly, which was calibrated using the following transitions: coesite–stishovite [24], α–β Mg_2SiO_4 [25], β–γ Mg_2SiO_4 [26], and enstatite–$\beta-Mg_2SiO_4$–stishovite [27]. In all three experiments stepped graphite heaters were applied and temperatures were measured with type C thermocouples, with emf's uncorrected for pressure. The product consisted on small colorless grains of around 10-60 μm in size.

In order to confirm the phase purity of the LN-$ZnTiO_3$ samples we performed synchrotron X-ray Laue micro diffraction and micro fluorescence measurements, at beam line 12.3.2. of the ALS [28]. Fluorescence scans were performed using a Vortex-EM (Hitachi High-Technologies Science America, Inc.). For the two dimensional fluorescence maps a 1 s exposure per step was employed, and measurements were performed on a grid with step sizes $\Delta x = \Delta y = 2$ μm. The energy window for the Ti K_α-line at 4510.84 eV was set to 3936.61 − 5093.22 eV, while the energy window for Zn K_α at 8638.86 eV was from 7879.14 to 9377.70 eV. For the diffraction experiments, a polychromatic X-ray beam (10–24 keV) was focused to approximately 1 × 1 μm^2 (FWHM) by Kirkpatrick-Baez mirrors. Laue diffraction patterns were collected with a PILATUS 1M area detector in reflection geometry. The sample was inclined to the primary beam by 45° and the area detector set to 90°. Laue patterns were indexed and analyzed using XMAS v.6 [29].

High-pressure Raman spectroscopy and SHG experiments were carried out using a Boehler-Almax diamond-anvil cell (DAC) equipped with 350-μm culet diamonds and tungsten gaskets indented to 40 μm in thickness with holes of 130 μm. For each high-pressure experiment a single grain of around 10 μm thickness was placed inside the gasket hole together with a ruby chip to measure the pressure [30] and Ar as pressure transmitting medium. The Raman experiment was performed in quasi-backscattering configuration with a Renishaw (RM-1000) spectrometer equipped with a 1800 grooves/mm grating and a spectral resolution of around 2 cm^{-1}. The excitation source was a HeNe laser (λ = 633 nm) focused down to a 10-μm spot with a 20× long working distance objective. An edge filter was used to filter the laser allowing measurements above 100 cm^{-1}. The SHG intensities at $\lambda_{2\omega}$ = 527 nm were measured in transmission geometry using the setup described by Bayarjargal et al. [31].

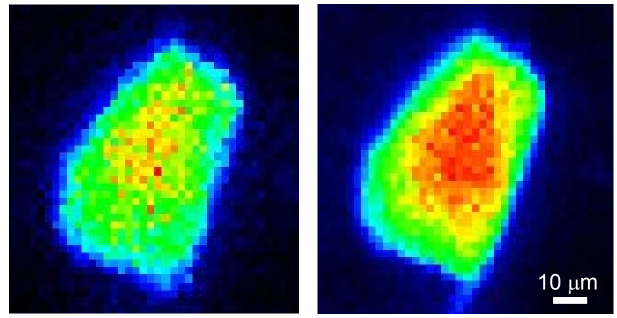

FIG. 1: Elemental distribution of Ti (left) and Zn (right) in a sample of $ZnTiO_3$. Variations in the fluorescence intensity are due to variations in the sample thickness.

III. *AB INITIO* CALCULATIONS

Ab initio calculations for LN-$ZnTiO_3$ and Pv-$ZnTiO_3$ were carried out at different pressures up to 25 GPa. We used a plane-wave pseudopotential approach to DFT as implemented in the CASTEP package [32]. Calculations were performed with either the PBE generalized gradient approximation [33] or the Wu-Cohen formulation [34] and either the norm-conserving pseudopotentials or the Vanderbilt Ultrasoft-type pseudopotentials from the "on the fly" data base of Accelrys Materials Studio 7. The reciprocal space was sampled according to the Monkhorst-Pack scheme [35] with a maximal distance of 0.03 Å^{-1} between the k-points and a plane-wave basis set with a kinetic energy cutoff of 1050 eV for the norm conserving pseudopotentials or 610 eV for the "on-the-fly" pseudopotentials. Variational density functional perturbation theory, DFPT, was used to evaluate the lattice dynamics and the response to an electric field [36] and the Raman intensities were computed as described in Milman et al. [37]. We complemented the calculations of the $ZnTiO_3$ polymorphs by calculations on LN-type $MgTiO_3$, $FeTiO_3$, and $MnTiO_3$, in order to validate the reliability of our computational approach. In the latter two cases, we employed a Hubbard U of 2.5 eV for the d-electrons of high-spin Fe^{2+} and Mn^{2+}.

IV. RESULTS AND DISCUSSION

A. Sample characterization

The fluorescence map showed the distribution of Zn and Ti in one of the synthesized grains of LN-type $ZnTiO_3$ (Fig. 1). The map showed a homogeneous distribution of the elements. No other elements were detected in the sample.

Out of the 1147 diffraction patterns obtained on a 31 × 37 mesh with 2 μm step size 520 were on the sample. Each frame typically contained about 100 to 230 reflections (Fig. 2) and we could index almost all reflections to the LN-type $ZnTiO_3$ phase using a two-grain model.

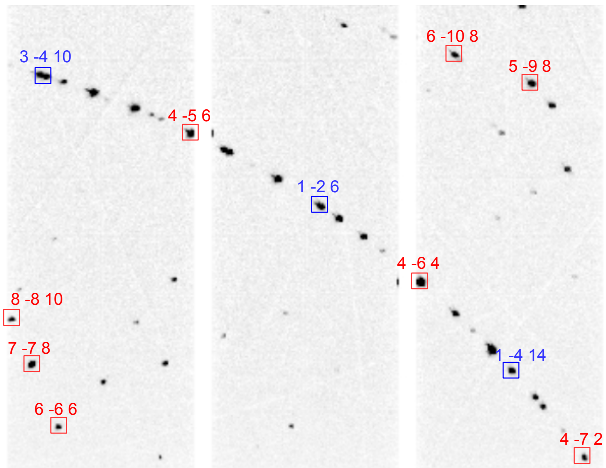

FIG. 2: Typical Laue diffraction pattern of the LN-type $ZnTiO_3$ sample. Nearly all reflections can be indexed using a two-grain model indicated by blue and red boxes, respectively. We only show some indeces for clarity.

This confirms that the sample consists of two crystalline domains of pure LN-$ZnTiO_3$.

B. Geometry optimization and phase stability

The Wu-Cohen exchange-correlation functional calculations on LN-type ATiO$_3$, with A = Mn, Mg, Fe or Zn gave lattice parameters in very good agreement (better than 0.5%) with experiment [12, 38–40]. The PBE-based calculations gave results which consistently showed the well-known underbinding. The full relaxed unit-cell parameters obtained from the calculation at ambient pressure for LN-type $ZnTiO_3$ are $a_{\text{theo}} = 5.2162$ Å and $c_{\text{theo}} = 13.9698$ Å. These unit-cell parameters are 2.4% and 1.8% larger than the experimental values obtained by Inaguna et al. [12] with powder x-ray diffraction, respectively.

In the case of Pv-$ZnTiO_3$ the calculation at 25 GPa yielded $a = 5.3330$ Å, $b = 7.5821$ Å, and $c = 5.1884$ Å as unit-cell parameters. From P-V curves we obtained a bulk modulus of 198 GPa, slightly smaller than the value reported for this phase of $ZnTiO_3$ in previous calculations (214 GPa) [12]. We found that the Pv-type phase of $ZnTiO_3$ is dynamically stable above 16 GPa, as then the frequencies of all modes are real, in good agreement with findings by Inaguna et al. [12].

C. Phonon dispersion curves

In LN-type compounds with point group C_{3v} the irreducible representation of the 20 modes at the zone center Γ are: $5\ A_1 + 5\ A_2 + 10\ E$. The two acoustic modes have $A_1 + E$ symmetry, the 5 A_2 modes are silent, and the remaining polar $4\ A_1 + 9\ E$ modes are Raman and infrared active. In the case of paraelectric Pv-$ZnTiO_3$

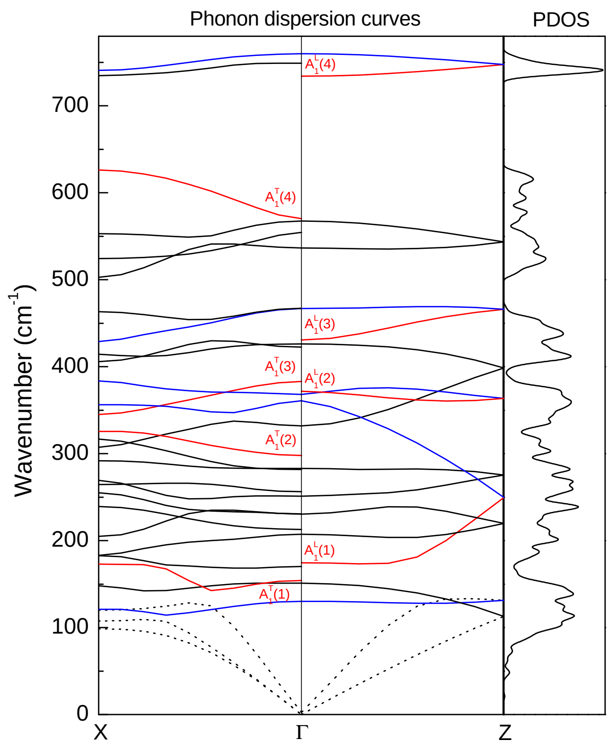

FIG. 3: Phonon dispersion curves of ferroelectric $LiNbO_3$-type $ZnTiO_3$ along the main symmetry directions of the Brillouin zone at 1 atm. The branches that correspond to the transversal-optic A_1^T and longitudinal-optic A_1^L modes are in red, the black lines correspond to the E modes, the blue lines correspond to the silent A_2 modes, and the dashed lines correspond to the acoustic branches. The right panel shows the corresponding phonon density of states (PDOS).

with point group D_{2h} there are 52 modes at the Γ point: $7\ A_g + 5\ B_{1g} + 7\ B_{2g} + 5\ B_{3g} + 10\ B_{1u} + 8\ B_{2u} + 10\ B_{3u}$. Three of these modes are acoustic $(B_{1u} + B_{2u} + B_{3u})$, the 24 even ($g$) modes are Raman active and the remaining 25 odd (u) modes are infrared active.

In a recent study, Inaguna et al. [12] report the calculated phonon dispersion of LN-$ZnTiO_3$. In ionic crystals, such as LN-$ZnTiO_3$, the electric field splits the transversal (TO) and longitudinal (LO) components of the A_1 and E polar modes. However, Inaguna et al. [12] report phonon branches at Γ that do not split and range up to 1770 cm^{-1}. A comparison to previous experimental values obtained for LN-$MgTiO_3$ and LN-$MnTiO_3$ [15, 40] implies that a phonon spectrum expanding to such high frequencies for LN-$ZnTiO_3$ is not realistic. In order to address this controversy we have repeated the phonon dispersion calculations for LN-$ZnTiO_3$. The result is shown in Fig. 3, together with the corresponding one-phonon density of states (PDOS).

The phonon branches have been calculated along the two high-symmetry directions $X\Gamma$ and ΓZ of the reciprocal space. The PDOS extends up to 760 cm^{-1}. When comparing the dispersion curves of LN-$ZnTiO_3$

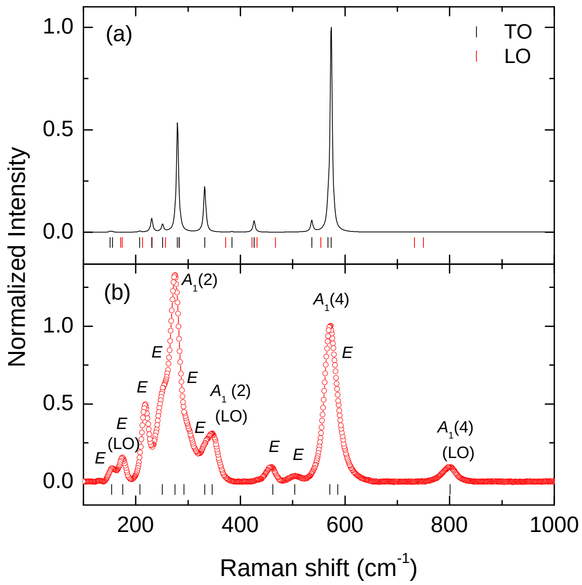

FIG. 4: (a) Calculated spectrum of $LiNbO_3$-type $ZnTiO_3$ at 1 atm. The frequencies of the TO (black ticks) and LO (red ticks) are shown. (b) The experimental spectrum of $LiNbO_3$-type $ZnTiO_3$ at 1 atm is shown together with the mode assignment made after comparing calculation and experiment. The ticks represent the frequencies of the experimentally observed modes.

with those of $LiNbO_3$ [41], one can see that there is some similarity despite a mode sequence change. The LO-TO splitting is shown in Fig. 3. Similarly to $LiNbO_3$ [41], in LN-$ZnTiO_3$, the A_1^T modes correspond to phonon branches that point from the xy (X point) hexagonal plane to the Γ point of the Brillouin zone and the A_1^L correspond to the same phonon branches but pointing to Γ from the z-axis. The E modes remain doubly degenerate along ΓZ and split to E^T and E^L along the $X\Gamma$ direction.

D. Raman Spectroscopy

The Raman spectra of LN-type compounds differing from $LiNbO_3$ or $LiTaO_3$ [42] have been previously reported for LN-$MgTiO_3$ and LN-$MnTiO_3$ [15, 40]. However, the continuous character of the spectrum, that consists of broad overlapping bands, and the lack of single crystals to separate the TO modes from the LO modes, which tend to mix, has prevented any Raman modes assignment. Here, we intend to assign the Raman modes of LN-$ZnTiO_3$ using powder samples. We have investigated the mode assignment by comparing the experimental and calculated Raman spectra as shown in Fig. 4.

The calculated Raman spectrum of LN-$ZnTiO_3$ is shown in Fig. 4 (a). It was computed by convoluting the sharp spectrum with a Lorentzian function with FWHM of 5 cm^{-1}, and does not show the LO modes due to an implementation restriction in our calculation. Despite of the narrow calculated bands and although the intensity of the LO modes is zero, the calculated spectrum shows that at least 6 of the 13 Raman active modes overlap. Even though there is a substantial broadening of the experimentally determined spectrum [Fig. 4 (b)] and we observe both LO and TO modes experimentally, the relative intensities in the experimentally determined and the computed Raman spectra are in very reasonable agreement. Hence, we could unequivocally identify 9 out of 13 TO modes of LN-$ZnTiO_3$ where the frequency mismatch between calculated and experimental values was $< 6\%$ for all modes. The agreement between theory and experiment is worse for the LO modes. We have assigned 4 of the 13 LO modes that should be present but for two of the modes (346 and 801 cm^{-1}) the frequency mismatch is above 7%. The frequencies and symmetry of the Raman modes of LN-$ZnTiO_3$ are shown in Table I. According to the calculations, the modes of LN-$ZnTiO_3$ that have not been experimentally observed are expected to be weak and to overlap strongly with the neighboring modes. In order to confirm our mode assignment we have studied the high-pressure Raman spectrum of LN-$ZnTiO_3$. If the mode assignment that we have made was correct, there should be an agreement between the experimental and calculated pressure coefficients of the modes. In Fig. 5 we show the evolution of the Raman spectra of LN-$ZnTiO_3$ for pressures up to 34.8 GPa.

The frequencies of the 9 TO and 4 LO modes of LN-$ZnTiO_3$ which we could identify at ambient pressure can be determined on pressure increase up to 20.8 GPa, when additional bands emerge. On increasing pressure all modes blueshift except the $A_1(2)$ mode at 275 cm^{-1} that redshifts up to $\sim$ 9 GPa when it overlaps with a neighboring E mode. We shall discuss the behavior of the soft mode in detail below. We interpret the appearance of additional Raman modes at 20.8 GPa as the onset of a phase transition that is completed below 24.6 GPa when the Raman bands assigned to the low-pressure phase have completely vanished. Based on our and previous *ab initio* calculations that predict a structural phase transition of LN-$ZnTiO_3$ at around 16 GPa to a Pv-type orthorhombic structure with space group $Pmna$ [12], we conclude that at 20.8 GPa LN-$ZnTiO_3$ begins to transform to Pv-$ZnTiO_3$. This is in contrast to the behavior of $LiNbO_3$, that has been found to become amorphous above 31 GPa [43], but it is well known that a non-hydrostatic environment can drastically shift transition pressures or induce amorphisation. The tick marks in Fig. 5 indicate the calculated and experimental frequencies of the modes at 24.6 GPa in the Pv-type phase. Though the broadening of the modes prevents an unambiguous assignment of the Raman modes for the Pv-type phase, some of the modes can be tentatively identified. The experimental and calculated frequencies of the Raman modes of the high-pressure phase are shown in Table I.

The pressure dependencies of the frequencies of the experimentally determined modes of LN-$ZnTiO_3$ up to 34.8 GPa is illustrated in Fig. 6. As stated before,

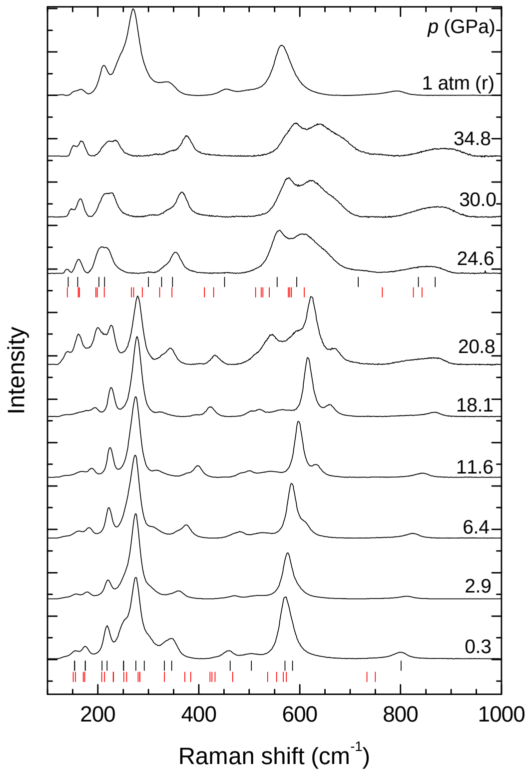

FIG. 5: Raman spectra at different pressures of $LiNbO_3$-type $ZnTiO_3$ and its high-pressure phase. The ticks indicate the positions of the experimental (black) and calculated (red) frequency of the modes.

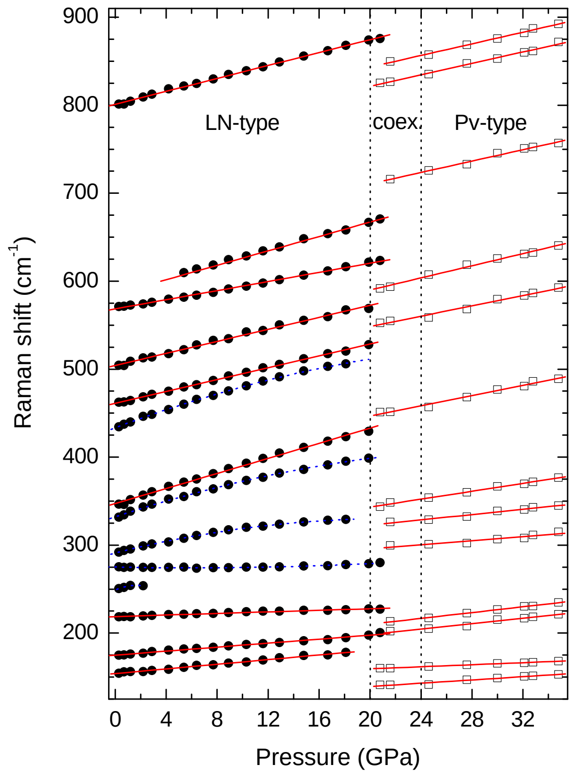

FIG. 6: Pressure dependence of the experimentally observed modes of the low-pressure and high-pressure phases of $ZnTiO_3$. The red solid lines are linear fits while the dashed blue lines are quadratic fits. The coexistence range (coex.) of both phases is indicated.

we can observe that the frequency of all modes in the low-pressure phase increases with pressure while the frequency of the $A_1^T(2)$ mode decreases. For those modes that linearly depend on pressure, the pressure coefficients are $a_i = \mathrm{d}\omega_i/\mathrm{d}P$, while for those that follow a quadratic behavior (modes at 251, 275, 292, 332, and 433 cm^{-1}), the pressure coefficients have been obtained from the low-pressure linear parts. The results are shown in Table I, where they are compared to the results of the model calculations.

Fig. 6 shows that the high-frequency modes of both phases have pressure coefficients that are around three times larger than those of the low-frequency modes. The agreement between the experimental and the calculated pressure coefficients of both the observed LO and TO modes is generally very good for LN-$ZnTiO_3$ where the softening of the $A_1^T(2)$ is also predicted by our *ab initio* calculations. Only the experimental pressure coefficient of the highest frequency $A_1^T(4)$ mode is in disagreement with the results of our model calculations, but due to a severe overlap with the highest-frequency E^T mode the experimentally determined value is rather uncertain. For Pv-$ZnTiO_3$ (Table II) the agreement between the pressure coefficients of the experimentally observed modes and the calculated modes is also very good. The good agreement of the pressure coefficients strongly supports

TABLE I: Experimental and calculated values for the zero-frequency (ω_0), and linear pressure coefficients a_i for the zone center TO (T) and LO (L) modes of LN-$ZnTiO_3$ at 1 atm obtained from high-pressure Raman scattering measurements and *ab initio* calculations. Raman modes ω and their pressure coefficients a_i are expressed in cm^{-1} and cm^{-1} GPa^{-1}, respectively.

	Exp.		Calc.			Exp.		Calc.	
Mode	ω_0	a_i	ω_0	a_i	Mode	ω_0	a_i	ω_0	a_i
E^T	154	1.3	151	1.1	E^L	175	1.1	171	0.8
$A_1^T(1)$			155	0.6	$A_1^L(1)$			174	0.1
E^T	218	0.5	207	0.8	E^L			213	0.4
E^T			230	1.3	E^L			231	1.3
E^T	251	1.2	251	1.1	E^L			257	1.0
$A_1^T(2)$	275	-0.1	280	-0.9	$A_1^L(2)$	346	4.3	372	4.8
E^T	292	3.0	283	4.3	E^L			283	4.6
E^T	332	3.8	332	3.4	E^L			422	3.7
$A_1^T(3)$			384	3.9	$A_1^L(3)$			431	0.3
E^T			426	4.1	E^L	462	3.4	467	3.4
E^T	504	3.4	537	3.8	E^L			554	2.3
E^T	586	4.1	567	3.2	E^L			750	3.5
$A_1^T(4)$	571	2.6	574	1.1	$A_1^L(4)$	801	3.7	733	3.8

TABLE II: Experimental and calculated values for the zero-frequency (ω_0) and linear pressure coefficients a_i of the Raman active modes of Pv-$ZnTiO_3$ at 25 GPa obtained from high-pressure Raman scattering measurements and *ab initio* calculations. Raman modes ω and their pressure coefficients a_i are expressed in cm^{-1} and cm^{-1} GPa^{-1}, respectively.

	Exp. (24.6 GPa)		Calc. (25 GPa)	
Mode	ω_0	a_i	ω_0	a_i
A_g	141	0.9	140	0.8
B_{2g}	162	0.6	161	0.7
B_{3g}			163	1.1
A_g	205	1.5	196	1.3
B_{1g}			199	0.9
B_{2g}	217	1.7	213	1.4
B_{1g}			266	0.9
A_g			271	1.0
B_{2g}	301	1.2	288	1.5
B_{3g}	329	1.5	322	0.9
A_g	354	2.2	347	1.8
B_{2g}			411	1.3
B_{1g}	457	2.9	430	2.6
A_g			512	2.8
A_g			524	2.3
B_{3g}			527	2.3
B_{2g}			540	2.7
B_{2g}	559	2.9	578	3.2
B_{3g}			581	3.3
B_{1g}			583	3.6
A_g	608	3.5	609	3.6
B_{1g}	726	3.2	764	3.6
B_{2g}	835	3.2	825	3.3
B_{3g}	876	3.3	849	3.4

our mode assignments.

We have commented in the introduction that in LN-type compounds the ferroelectric ($R3c$) phase can be transformed to the paraelectric ($R\overline{3}$) phase by one A_1 soft mode. However, this $R3c \rightarrow R\overline{3}$ transformation would also require an octahedral tilting, which is not allowed by symmetry in $R\overline{3}$, and thus there is an order-disorder $R3c \rightarrow Pnma$ transition instead, such as has already been observed for LN-$ZnTiO_3$. In $LiNbO_3$, this soft mode is the lowest-frequency $A_1(1)$ mode which consists of an antiphase vibration of the Nb atoms against the O framework along the c-axis, while the Li atoms are not displaced. This anharmonic [20] mode has been controversially observed to soften at high temperature by some authors [44] in $LiNbO_3$. Under high pressure its frequency barely shifts, showing an experimental pressure coefficient close to zero [21].

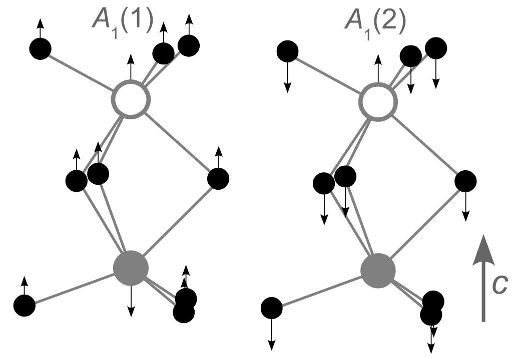

FIG. 7: Connected TiO_6 and ZnO_6 ocathedra of $ZnTiO_3$ in the $LiNbO_3$-type structure showing the eigenvectors of the $A_1(1)$ and $A_1(2)$ Raman modes. The empty, full gray, and black circles represent the Ti, Zn, and O atoms, respectively. The black arrows show the displacement.

One would expect a similar behavior of the $A_1(1)$ mode of LN-$ZnTiO_3$. However, although we have not been able to detect the $A_1(1)$ mode by Raman spectroscopy, our calculations show that the frequency of this mode (155 cm^{-1}) blueshifts with a pressure coefficient of 0.6 cm^{-1} GPa^{-1}. In order to better understand the difference between the $A_1(1)$ mode of $LiNbO_3$ and LN-$ZnTiO_3$ we have shown in Fig. 7 the calculated eigenvectors of the $A_1(1)$ and $A_1(2)$ modes of LN-$ZnTiO_3$. In contrast to $LiNbO_3$, in LN-$ZnTiO_3$ the $A_1(1)$ mode consists on an in-phase vibration of the Ti and O atoms along the c axis with the Zn atoms vibrating in antiphase also along the polar axis as in the $A_1(2)$ mode of $LiNbO_3$. However, the $A_1(2)$ mode of LN-$ZnTiO_3$ is, similarly to the $A_1(1)$ mode of $LiNbO_3$, an antiphase vibration of the Ti atoms against the oxygen framework with the Zn atoms at rest. In $LiNbO_3$ the $A_1(1)$ mode has a frequency of 256 cm^{-1}, slightly smaller than that of the $A_1(2)$ mode of LN-$ZnTiO_3$ (275 cm^{-1}), as expected by the larger atomic mass of Nb compared to Ti. However, the $A_1(1)$ of LN-$ZnTiO_3$ and the $A_1(2)$ mode of $LiNbO_3$ involve the Zn and the 10 times lighter Li atoms, respectively. This results in a frequency 50% larger for this mode in $LiNbO_3$ [45]. The strong compositional dependence of the frequencies of the two low-frequency A_1 modes of LN-$ZnTiO_3$ and $LiNbO_3$ explains why in LN-$ZnTiO_3$ it is the $A_1(2)$ and not the $A_1(1)$ mode that softens under pressure (Table I). This should also be the case in other LN-type compounds where the A cation is a transition metal, but the lack of detailed Raman spectroscopic studies currently prevents a confirmation of this conclusion. Our findings agree with previous calculations [20, 46] performed on $LiNbO_3$, where the atomic mass of Li can be neglected in comparison to the atomic mass of Nb.

E. Second Harmonic Generation

According to Inaguna et al. [12], the intensity of SHG signal ($I_{2\omega}$) of LN-$ZnTiO_3$ is up to 24 times larger than that of $ZnSnO_3$, which facilitates high-pressure experiments. We have shown earlier that high-pressure SHG measurements are an excellent approach to characterize powder samples [47]. Fig. 8 shows the variation of the normalized $I_{2\omega}$ with pressure. $I_{2\omega}$ remains constant up to ≈20 GPa when it starts to decrease as a consequence of the ferroelectric to paraelectric transformation to a centrosymmetric space group ($Pmna$), in good agreement with the results of the Raman spectroscopic measurements described above and previous *ab initio* calculations [12]. The Raman data implied a first order transition, where both phases coexisted in a pressure interval of about 4 GPa up to around 24 GPa. This is consistent with the pressure dependence of the SHG signal, which disappears at around 24 GPa. Non-phase matchable materials are those materials with a non centrosymmetric structure in which the excitation wave (with wavelength ω) and the generated SHG wave (with wavelength 2ω) propagate with different phase velocities. Therefore, the intensity of the generated SHG signal is usually many orders of magnitude lower than the intensity of the fundamental wave. In the case of phase matchable materials an effective conversion from the incident photons to SHG is possible by the appropiate choice of the crystal orientation and polarization fields [47]. We have shown earlier that for phase matchable crystals $I_{2\omega}$ is independent of the grain size when the latter exceeds a critical diameter [47]. The application of pressure will cause a decrease of the grain size, and only in the case of a phase matchable sample with large grains $I_{2\omega}$ would be independent of the pressure. For phase matchable materials with small grains, pressure would lead to either independence or a decrease of $I_{2\omega}$, while for non-phase matchable compounds $I_{2\omega}$ would either increase or decrease, depending on whether the grain size is below or above a compound-specific diameter. For phase-matchable $LiNbO_3$ the critical size is about 50 μm [47]. From the diffraction experiments we know that the synthesized grains of $ZnTiO_3$ used in our experiments consist on single-crystal domains with diameters of $\sim$ 30 μm, and so the combination of our experimental approaches strongly implies that $ZnTiO_3$ is a phase matchable material.

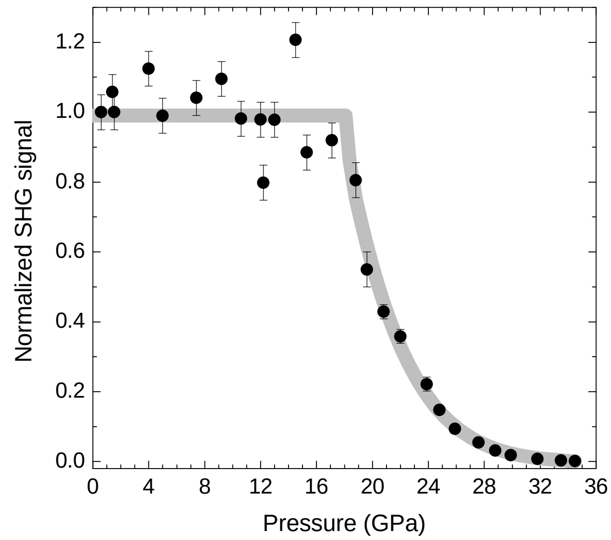

FIG. 8: Pressure dependence of the normalized second harmonic generation (SHG) signal.

V. SUMMARY AND CONCLUSIONS

The properties and stability of ferroelectric $LiNbO_3$(LN)-type $ZnTiO_3$ have been studied under high pressure up to 34.8 GPa across the ferroelectric to paraelectric phase transition. Raman spectroscopy and second harmonic generation (SHG) studies reveal that the phase transition starts at 20 GPa in agreement with previous calculations. *Ab initio* lattice dynamic calculations have been employed to assign the symmetries of most LO and TO Raman active modes of the ferroelectric ($R3c$) and paraelectric ($Pmna$) phases and to determine the phonon branches in the $X\Gamma$ and ΓZ directions of the Brillouin zone of LN-$ZnTiO_3$. The calculated one-phonon density of states (PDOS) shows that the phonon spectrum of LN-$ZnTiO_3$ extends up to 760 cm^{-1}. The $A_1(2)$ mode of LN-$ZnTiO_3$ has been found to soften under pressure with a pressure coefficient of -0.1 cm^{-1} GPa $^{-1}$. Our calculations show that the polarisation vector of this mode is an antiphase vibration of the Ti cations against the O framework along the c axis while the Zn cations stay at rest. This is similar to the ferroelectric soft mode of perovskites. We have also found that the frequency of the $A_1(1)$ mode of LN-$ZnTiO_3$, which consists of the in-phase vibration of the Ti cations and the oxygen framework along the c axis while the Zn cations vibrate in antiphase, and the frequency of the $A_1(2)$ mode are swapped with respect to $LiNbO_3$. While the ferroelectric soft mode of $LiNbO_3$, $A_1(1)$, presents a similar frequency to the ferroelectric $A_1(2)$ mode of LN-$ZnTiO_3$, the $A_1(1)$ mode of LN-$ZnTiO_3$ is 50% larger than the frequency of the $A_1(2)$ mode of $LiNbO_3$. We explain this by the contribution of the A cation on the $A_1(1)$ and $A_1(2)$ modes of LN-$ZnTiO_3$ and $LiNbO_3$, respectively, with Zn being ten times more massive than Li. This result shows that independently of the relative atomic masses of the A and B cations in these ferroelectric compounds, the contribution of the displacement of the A cations is negligible in the ferroelectric instability and that the displacement of the B cations plays the most important role in LN-type compounds. Finally, SHG experiments were employed to qualitatively follow the pressure-induced change of the spontaneous polarization. This has allowed us to confirm the nature of the ferroelectric to paraelectric phase transition of LN-$ZnTiO_3$ and conclude that polar

$ZnTiO_3$ is a phase matchable material.

Acknowledgments

We thank Andreas Ebert for his support during the multi-anvil experiments. J.R.-F. thanks the Alexander von Humboldt Foundation for a postdoctoral fellowship. B.W. and W.M. acknowledge financial support from the BMBF project number 05K13RF1. The Advanced Light Source (ALS) is supported by the Director, Office of Science, Office of Basic Energy Sciences, of the U.S. Department of Energy under Contract No. DE-AC02-05CH11231 at the Lawrence Berkeley National Laboratory (LBNL).

---

[1] G. Catalan and J. F. Scott, Adv. Mater. **21**, 2463 (2009).
[2] J. B. Neaton, C. Ederer, U. V. Waghmare, N. A. Spaldin, and K. M. Rabe, Phys. Rev. B. **130**, 014113 (2005).
[3] R. Resta, Modell. Simul. Mater. Sci. Eng. **11**, R69 (2003).
[4] G. Saghi-Szabo, R. E. Cohen, and H. Krakauer, Phys. Rev. Lett. **80**, 4321 (1998).
[5] J. F. Scott and C. A. Paz de Araujo, Science **246**, 1400 (1989).
[6] G. Binnig, C. F. Quate, and C. Gerber, Phys. Rev. Lett. **56**, 930 (1986).
[7] P. J. Muralt, Micromech. Microeng. **10**, 136 (2000).
[8] N. Takashi, N. Yuichi, K. Akira, and T. Hidemi, Appl. Phys. Lett. **65**, 1522 (1994).
[9] B. Noheda, J. A. Gonzalo, L. E. Cross, R. Guo, S. E. Park, D. E. Cox, and G. Shirane, Phys. Rev. B **61**, 8687 (2000).
[10] Y. Inaguna, M. Yoshida, and T. Katsumata, J. Am. Chem. Soc. **130**, 6704 (2008).
[11] Y. Inaguna, M. Yoshida, T. Tsuchiya, A. Aimi, K. Tanaka, T. Katsumata, and D. Mori, J. Phys: Conf. Series **215**, 012131 (2010).
[12] Y. Inaguna, A. Aimi, Y. Shikaro, D. Sakurai, D. Mori, H. Kojitani, M. Akaogi, and M. Nakayama, J. Am. Chem. Soc. **136**, 2748 (2014).
[13] D. Vanderbildt, Curr. Opin. Solid State Mater Sci. **2**, 701 (1997).
[14] N. A. Benedek and C. J. Fennie, J. Phys. Chem. C **117**, 13339 (2013).
[15] X. Wu, S. Qin, and L. Dubrovinsky, Geoscience Frontiers **2**, 107 (2011).
[16] N. C. Wilson, S. P. Russo, J. Muscat, and N. M. Harrison, Phys. Rev. B **72**, 024110 (2005).
[17] H. Gou, J. Zhang, Z. Li, G. Wang, F. Gao, R. C. Ewing, and J. Lian, Appl. Phys. Lett. **98**, 091914 (2011).
[18] W. Wang, S. Wang, D. He, and J. Xu, Solid State Commun. **196**, 8 (2014).
[19] A. V. Postnikov, T. Neumann, and G. Borstel, Phys. Rev. B **50**, 758 (1994).
[20] V. Caciuc, A. V. Postnikov, and G. Borstel, Phys. Rev. B **61**, 8806 (2000).
[21] J. Mendes Filho, V. Lemos, and F. Cerdeira, J. Raman Spec. **15**, 367 (1984).
[22] M. R. Tejerina, K. Pereira da Silva, A. R. Goñi, and G. A. Torchia, Optical Materials **36**, 581 (2013).
[23] T. Bernert, J. Ruiz-Fuertes, L. Bayarjargal, and B. Winkler, Solid State Sciences **43**, 53 (2015).
[24] M. Akaogi, H. Yusa, K. Shiraishi, and T. Suzuki, J. Geophys. Res. **100**, 337 (1995).
[25] H. Morishima, T. Kato, M. Suto, E. Ohtani, S. Urakawa, W. Utsumi, O. Shimomura, and T. Kikegawa, Science **26**, 1202 (1994).
[26] T. Inoue, D. J. Weidner, P. A. Northrup, and J. P. Parise, Earth Planet. Sci. Lett. **160**, 107 (1998).
[27] T. Gasparik, Contrib. Mineral. Petr. **102**, 389 (1989).
[28] M. Kunz, N. Tamura, K. Chen, A. A. MacDowell, R. S. Celestre, M. M. Church, S. Fakra, E. E. Domning, J. M. Glossinger, J. L. Kirschman, et al., Rev. Sci. Instrum. **80**, 035108 (2009).
[29] N. Tamura, in *Strain and Dislocation Gradients from Diffraction*, edited by R. Barabash and G. Ice (Imperial College Press (London), 2014), pp. 125–155.
[30] H. K. Mao, P. M. Bell, J. W. Shaner, and D. J. Steinberg, J. Appl. Phys. **49**, 3276 (1978).
[31] L. Bayarjargal, B. Winkler, E. Haussühl, and R. Boehler, Appl. Phys. Lett. **95**, 061907 (2009).
[32] S. J. Clark, M. D. Segall, C. J. Pickard, P. J. Hasnip, M. J. Probert, K. Refson, and M. C. Paynei, Z. Kristallogr. **220**, 567 (2005).
[33] J. P. Perdew, K. Burke, and M. Ernzerhof, Phys. Rev. Lett. **77**, 3865 (1996).
[34] Z. Wu and R. Cohen, Physical Review B **73** (2006).
[35] H. J. Monkhorst and J. D. Pack, Phys. Rev. B **13**, 5188 (1976).
[36] K. Refson, P. Tulip, and S. Clark, Physical Review B **73**, Art. Nr 155114 (2006).
[37] V. Milman, A. Perlov, K. Refson, S. J. Clark, J. Gavartin, and B. Winkler, J. Phys.: Condens. Matter **21**, 485404 (2009).
[38] N. L. Ross, J. Ko, and C. T. Pewitt, Phys. Chem. Minerals **16**, 621 (1989).
[39] K. Leinenweber, W. Utsumi, Y. Tsuchida, T. Yagi, and K. Kurita, Phys. Chem. Miner. **18**, 244 (1991).
[40] J. A. Linton, Y. Fei, and A. Navrotsky, Am. Mineral. **84**, 1595 (2008).
[41] K. Parlinski, Z. Q. Li, and Y. Kawazoe, Phys. Rev. B **61**, 272 (2000).
[42] A. Jayaraman and A. A. Ballman, J. Appl. Phys. **60**, 1208 (1986).
[43] Y. Lin, Y. Li, Y. Xu, G. Lan, and H. Wang, J. Appl. Phys. **77**, 3584 (1995).
[44] A. S. Backer, A. A. Ballman, and J. A. Ditzenberger, Phys. Rev. B **2**, 4233 (1970).
[45] A. Ridah, P. Bourson, M. D. Fontana, and G. Malovichko, P. Phys.: Condens. Matter. **9**, 9687 (1997).
[46] I. Inbar and R. E. Cohen, Phys. Rev. B **53**, 1193 (1996).
[47] L. Bayajargal and B. Winkler, Z. Kristallogr. **229**, 92 (2014).